Microstructure and mechanical properties of WC or Mo_2C modified NbC-Ni cermets

J. H. Huang[a*], S. G. Huang[a], P. Zhou[b], B. Lauwers[c], J. Qian[c], J. Vleugels[a]

[a] Department of Materials Engineering, KU Leuven, Belgium

[b] Hunan Provincial Key Defense Laboratory of High Temperature Wear-Resisting Materials and Preparation Technology，Hunan University of Science and Technology, China

[c] Department of Mechanical Engineering, KU Leuven and Member Flanders Make, Belgium

Abstract

In this study, the influence of up to 15 vol% WC or Mo_2C addition to Ni bonded NbC matrix cermets, prepared by pressureless liquid phase sintering in vacuum for 90 min at 1390 °C was assessed. The constituent phases and W/Mo dissolution in the Ni binder and NbC phases were simulated by thermodynamic modelling. Microstructure and phase analysis using XRD and SEM indicated that the WC or Mo_2C modified NbC based cermets were composed of a (Nb,W)C or (Nb,Mo)C solid solution cubic phase dispersed in a cubic Ni alloy binder. Residual WC was present in the cermets with ≥10 vol% WC addition, whereas up to 15 vol% Mo_2C addition completely dissolved into the NbC cermets. The phase evolution and influence of the WC/Mo_2C content on the solid solution formation is discussed and the fracture toughness, Vickers hardness and transverse rupture strength was assessed.

Key words: Niobium carbide, Cermets, Liquid phase sintering, Microstructure, Mechanical properties

1. Introduction

Cemented carbides based on tungsten carbide (WC) with a cobalt (Co) binder phase are widely used as cutting tools due to their extremely favourable combination of hardness, toughness, wear-resistance and strength[1,2]. Secondary carbides such as NbC, TaC, Cr_3C_2, Mo_2C, etc, were added to WC-Co based cemented carbides to tailor the mechanochemical properties for specific applications[3]. During use, WC-Co cemented carbides could be easily transformed into a submicron particle size oxide mixture of $CoWO_4$ and WO_3 by oxidation and wear processes[4]. The formation of water soluble WO_3 upon oxidation, and the high solubility of WC in Fe-based alloys at

elevated temperatures favoured abrasive and especially dissolution crater wear[5-7]. The maximum application temperature of WC-Co cemented carbides was 800 to 900 °C. At higher temperatures, plastic deformation due to softening of the binder phase and the reaction between WC and Co led to tool failure[9].

Extensive research had been devoted to the possible replacement of WC by other carbides or carbonitrides, such as niobium carbide (NbC) and titanium carbonitride (TiC_xN_{1-x}). Niobium oxide (Nb_2O_5) from the oxidized NbC had fully REACH-registered and no particular hazards or critical notifications for Nb_2O_5 and NbC were filed so far[10]. The solubility of NbC in iron, cobalt and nickel was substantially lower than that of WC at elevated temperatures[11], resulting in reduced crater wear of NbC inserts when dry cutting these alloys. The melting temperature of NbC was higher than that of WC, the hot hardness could be tailored exceeding that of WC above 600 °C and the E-modulus and hardness of NbC were quite stable with increasing temperature[10]. Huang et al. [12] investigated the influence of the Co content on the mechanical properties and microstructure of NbC-Co cermets prepared by Spark Plasma Sintering. The effect of WC, Mo_2C, VC and Mo on the NbC grain growth, microstructure evolution and mechanical properties was investigated, and demonstrated that the addition of secondary carbides improved the binder/NbC wettability and minimized NbC grain growth with a Ni or Co binder[12-15]. NbC grain growth inhibition was achieved by adding Al to a NbC-Fe alloy or by adding Mo_2C or VC to a NbC-Ni cermet[16]. However, the mechanical properties, i.e. hardness and flexural strength of NbC-Ni based cermets was modest due to an apparent grain growth. Therefore, secondary carbides wereintroduced into NbC-Ni systems as microstructure modifiers to improve their mechanical properties for different applications. It was well known that Mo_2C or Mo was used as sintering aid to improve the wettability of hard phases like TiC or Ti(C,N) and metallic binder phases[17, 18]. WC was a necessary component in Ti(C,N) based cermet systems to improve mechanical properties[19]. A core-rim structure wasreported in NbC-Ni based cermets with WC addition[15]. However, the core-rim structure evolution with the WC content and its formation mechanism needs to be further investigated.

The wettability between binder and carbide phase was important during liquid phase sintering of hardmetals[20]. The microstructure of a hot pressed NbC-24.5 wt.% Co with WC addition was characterized by a relatively continuous, interconnected and irregular NbC grain network with an isolated Co binder phase, indicating a poor

wettability of NbC by the Co binder[21]. A much better wetting between NbC and Ni binder in NbC-Ni with different fractions of Al metal powder was observed during conventional liquid phase sintering in vacuum[9]. Fe_3Al was also used as a binder to improve the strength and toughness of sintered NbC[22]. In addition, Ni bonded NbC cermets represented a viable alternative to Co bonded WC[14]. Nb is known to be one of the most biocompatible metals, whereas Ni powder does not have the same hazardous classification as Co powder[10]. In this study, Ni was chosen as binder phase due to its good wetting behaviour with cubic carbides.

Thermodynamic factors make solid-state sintering difficult for most hard materials and the most widely applied sintering method is liquid phase sintering[23]. In this paper, NbC-10Ni (vol%) powders with various amounts of WC or Mo_2C additions were sintered to full density via liquid phase sintering. The effects of the added amount of WC/Mo_2C on the density, microstructure, hardness, fracture toughness and transverse rupture strength were investigated and compared with the reference NbC-10Ni (vol%) bonded cermets.

2. Experimental details

NbC (CBMM, FSSS = 1.75 µm, Brazil), WC (Umicore, CW5300, FSSS = 2 µm, Belgium), Mo_2C (Langfeng, FSSS = 3.50 µm, China) and Ni (Vale, T123™, FSSS = 3-7 µm, UK) powders were used as starting materials. The NbC powder had total C and O contents of 11.2 and 0.17 wt%, respectively. The overall composition of the starting powder mixtures is summarized in Table 1. NbC-10Ni-(2.5 to 15) WC or (2.5 to 15) Mo_2C (vol%) powder mixtures were weighted and mixed on a multi-directional mixer (Turbula) for 48 h in ethanol using WC-6 wt% Co milling balls (Ceratizit, H20C). The ball-to-powder mass ratio was 5:1. After mixing, the powder suspensions were dried on a rotating evaporator at 75 °C. The dried powder mixtures were cold isostatically pressed into green cylinder blanks at 250 MPa for 2 min and sintered by conventional pressureless liquid phase sintering for 90 min at 1390 °C at a heating rate 3 °C /min in a dynamic vacuum (~ 20 Pa) in a graphite furnace (HP, W100/150-2200-50 LAX, FCT Systeme, Frankenblick, Germany). In order to investigate the core rim evolution in the WC doped cermets, NbC-10 Ni-15 WC (vol%) green compacts were sintered at different temperatures for 90 min and at 1390 °C for different dwell times.

The equilibrium phase diagram and constituent phase compositions were simulated by Thermo-Calc software using the TCFE10 database[13]. The density of the sintered cermets was measured in demineralized water using the Archimedes method. Cross-sectioned cermets were ground with a diamond plate using an aqueous 15 μm diamond suspension, then polished on canvas with 3 and 1 μm colloidal diamond aqueous suspension. The phases were identified by X-ray diffraction (XRD, Seifert 3003 T/T) on polished cross-sections of the cermets. In addition, the lattice parameters of the NbC and Ni phases were refined via Maud software based on the Rietveld method [24]. The micro-hardness (Model FV-700, Future-Tech Corp.,Tokyo) was measured with a load of 30 kg during 15 s. The reported values are the mean and standard deviation of five indentations. The Palmqvist indentation fracture toughness, K_{IC}, was assessed from the length of the radial cracks originating from the corners of these indentations and calculated according to the formula of Shetty[25]. Three point bending testing was conducted on planparallel ground 2.0x3.0x25.0 mm^3 specimens on an Instron 4467 with 1 kN load cell, a span length of 20 mm and a cross-head speed of 0.1 mm/s. The reported data are the average and standard deviation of 5 specimens.

The microstructure of polished cross-sections was observed by scanning electron microscopy (NanoSEM 450 and XL-30 FEG, FEI). Schematics diagrams of the core-rim structure of WC-doped cermets were coloured by PS CC2018 based on BSE images at a high magnification. The average NbC and Ni grain sizes were measured by EBSD at 800x magnification. EBSD analysis was carried out on a Philips XL30 SEM using OIM software for grain size analysis. A 20 kV accelerating voltage was used with 4x4 binning of the EBSD patterns and a step size of 0.2 μm. The grain core diameter and rim thickness of the core-rim carbide grains was obtained from their area, based on BSE micrographs assuming that a circular core with a surrounding ring rim. The contiguity of the carbide grains, C, was calculated by the following equation[26]:

$$C = \frac{2N_{NbC/NbC}}{2N_{NbC/NbC}+N_{NbC/Ni}} \quad (1)$$

where $N_{NbC/NbC}$ and $N_{NbC/Ni}$ represent the number of NbC/NbC and NbC/Ni interfaces respectively, obtained by the line intercept technique on BSE micrographs at 2000x magnification.

3. Results and Discussion

3.1. Thermodynamic predictions

The calculated equilibrium phase diagrams of the NbC-10Ni-WC/Mo_2C (vol%) systems, using Thermo-Calc and the TCFE10 database, are presented in Fig. 1. The content of WC and Mo_2C was varied from 2.5 to 15 vol%, corresponding to 4.84 to 25.89 wt% WC and 2.85 to 16.79 wt% Mo_2C, respectively. The selected compositions are indicated by the vertical lines in Fig. 1. In the phase diagrams, the stable phases were the metallic Ni binder with fcc structure, WC with hexagonal structure, (Nb,W)C or (Nb,Mo)C solid solution phase with fcc structure and $NbNi_3$ phase. The lowest temperature at which liquid phase was formed was close to 1302 °C for the WC/Mo_2C free cermets. The solidus temperature of the WC doped cermets initially increased from 1302 °C up to a maximum of 1315 °C at 9 wt% WC with increasing WC content and decreased again to 1312 °C when the solid solubility limit of WC in NbC was reached at 21 wt% WC. The solidus temperature for Mo_2C doped cermets decreased from 1302 °C to 1232 °C with increasing Mo_2C addition, and remained constant at this temperature. The liquid phase sintering temperature in NbC-12Ni-(3-9)Mo_2C (vol%), which was very close to the selected compositions, was measured to be around 1300 °C [27], and well below the applied sintering temperature of 1390 °C.

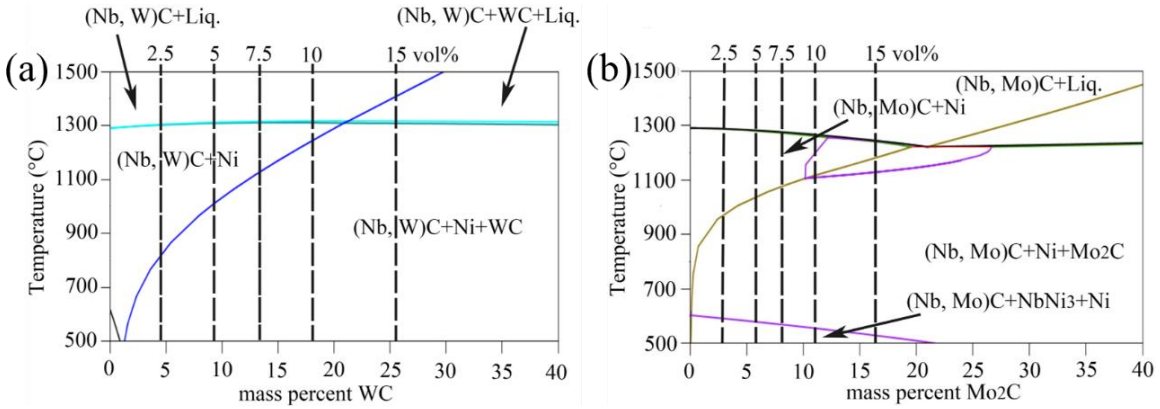

Fig. 1. Equilibrium phase diagrams for the (a) $NbC_{0.96}$-10Ni-xWC (vol%) and (b) $NbC_{0.96}$-10Ni-xMo_2C (vol%) cermets.

The calculated isothermal section of the NbC-WC-Mo_2C system at 1000°C, shown in Fig. 2(a), indicates that there is no liquid phase in the WC or Mo_2C doped cermets at 1000 °C. However, WC/Mo_2C and NbC partially dissolved into the Ni binder and WC/Mo_2C also dissolved into the NbC phase to form a solid solution (Nb,W/Mo)C and

Ni binder phase. Additionally, WC remained in > 5 vol% WC doped cermets at 1000 °C. Liquid phase was formed in all WC/Mo_2C doped cermets at 1390 °C indicating liquid phase sintering can be performed at this temperature, as shown in Fig. 2(b). All selected WC/Mo_2C compositions were located in the same phase field showing the presence of liquid Ni binder and (Nb,W/Mo)C due to the fact that the solid solubility was increased with increasing temperature. According to the Thermo-Calc calculation of the liquid binder and NbC phase composition, shown in Fig. 2(c) and 2(d) respectively, the amount of WC or Mo_2C that dissolved into the Ni metallic binder and the NbC phase linearly increases with increasing secondary carbide content in the starting powder, and reaches a maximum at 23 wt % WC or 33 wt % Mo_2C addition. The solubilities of NbC, WC and Mo_2C in nickel at 1400 °C were reported to be 7, 27 and 36 wt% respectively[28].

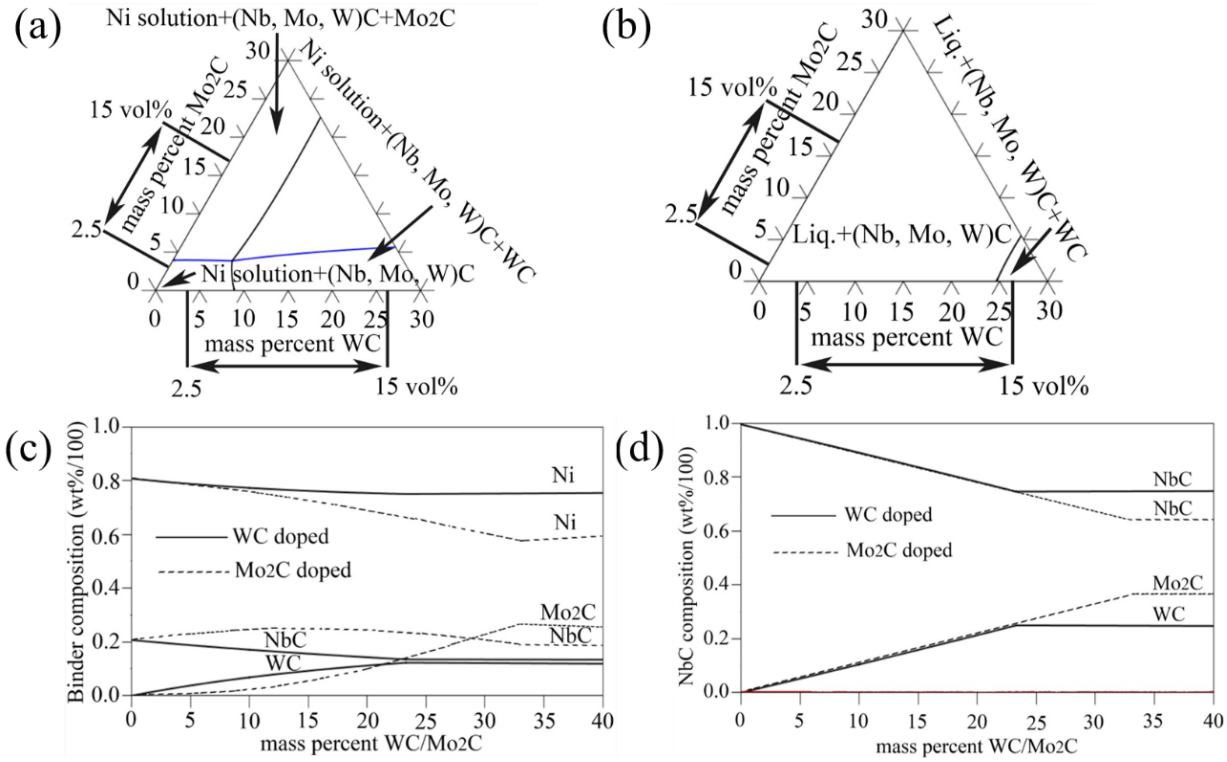

Fig. 2. Isothermal section of the $NbC_{0.96}$-10Ni-xWC/Mo_2C system at (a) 1000 °C and (b) 1390 °C. Calculated Ni binder phase (c) and NbC phase (d) composition at 1390 °C.

3.2. Constituent phases

The chemical compositions, along with the theoretical (TD) and measured (MD) density, of the investigated NbC-Ni based cermets are summarised in Table 1. The sintered density (MD) clearly followed the theoretical density and increased with the amount of added WC/Mo_2C. The theoretical density was calculated from the starting powder composition, assuming a density of 7.79, 8.91, 15.68 and 9.06 g/cm^3 for NbC, Ni, WC and Mo_2C respectively. All pressureless sintered cermets could be considered as fully dense.

Table 1 Chemical composition and density of the investigated NbC-Ni based cermets

Cermet (vol%)	Composition (wt%)	WC/Mo_2C (mol%)	TD (g/cm^3)	MD (g/cm^3)
WC influence				
NbC-10 Ni	NbC-11.27 Ni	0	7.92	7.92
NbC-10 Ni-2.5 WC	NbC-11 Ni-4.84 WC	2.43	8.10	8.10
NbC-10 Ni-5- WC	NbC-10.74 Ni-9.45 WC	4.87	8.30	8.33
NbC-10 Ni-7.5 WC	NbC-10.49 Ni-13.85 WC	7.29	8.49	8.51
NbC-10 Ni-10 WC	NbC-10.25 Ni-18.04 WC	9.70	8.69	8.72
NbC-10 Ni-15 WC	NbC-9.80 Ni-25.89 WC	14.49	9.08	9.13
Mo_2C influence				
NbC-10 Ni-2.5 Mo_2C	NbC-11.23 Ni-2.85 Mo_2C	1.37	7.93	7.91
NbC-10 Ni-5 Mo_2C	NbC-11.18 Ni-5.69 Mo_2C	2.76	7.97	7.95
NbC-10 Ni-7.5 Mo_2C	NbC-11.14 Ni-8.50 Mo_2C	4.18	8.00	7.98
NbC-10 Ni-10 Mo_2C	NbC-11.10 Ni-11.28 Mo_2C	5.62	8.03	8.02
NbC-10 Ni-15 Mo_2C	NbC-11.01 Ni-16.79 Mo_2C	8.60	8.09	8.06

The XRD patterns of the pure Ni different cermets with WC sintered at 1390 °C for 90 min are compared in Fig. 3(a, b, c). A diffraction peak of residual WC was clearly visible in the NbC-10Ni-10WC (vol%) and NbC-10Ni-15WC (vol%) compositions. The main diffraction peak of NbC gradually shifted to higher diffraction angles with increasing WC content, to reach a maximum shift at 7.5 vol% WC addition as shown

in Fig. 3(b), because of the solid solubility of W into the NbC lattice[29, 30]. The main diffraction peak of the Ni binder had shifted to a lower diffraction angle, compared to that of pure Ni, but the peak position in the cermets hardly changed as a function of the WC content. The sintered cermets were composed of a (Nb,W)C solid solution cubic phase dispersed in a cubic Ni alloy binder, along with a residual WC phase at starting powder WC contents ≥10 vol%. Although WC was predicted in all selected WC doped cermets at room temperature (see Fig. 1(a)), it was only observed in the 10 and 15 vol% WC doped cermets due to the slow outward diffusion from the (Nb,W)C matrix and concomitant precipitation during cooling down.

The diffraction patterns of the pure Ni and Mo_2C containing cermets are compared in Fig. 3(d, e, f). No Mo_2C diffraction peak was observed in any of the Mo_2C doped cermets, and only a Ni alloyed binder phase and a (Nb,Mo)C solid solution could be identified, as shown in Fig. 3(d). With increasing Mo_2C content, the Ni diffraction peak progressively shifted towards lower 2θ values and the opposite trend was observed for the diffraction peak of the (Nb,Mo)C phase as presented in Fig. 3(f) and (e). Complete solid solution of all selected Mo_2C compositions was achieved after 90 min at 1390 °C since Mo has a high solubility in the Ni binder and carbide phases, as reported for the TiC-18TiN-24Ni-(5-14)Mo_2C system[31]. The fact there was no $NbNi_3$ phase observed in the XRD patterns at room temperature in any of the Mo_2C doped cermets was inconsistent with the results of the calculated equilibrium phase diagram shown in Fig. 1(b). Only a carbide phase solid solution and nickel-rich binder were obtained in the NbC-12Ni-0.5WC-(0-9)Mo_2C (vol%) system after heating at 6 °C/min to 1450 °C and immediately cooled upon reaching 1450 °C at 20 °C/min to 20 °C in vacuum (5.10^{-6} bar)[27]. Mo_2C also precipitates at a very low temperature according to calculated phase diagram, but Mo_2C could not be detected in the XRD patterns. The 2θ shift of the NbC and Ni diffraction peaks in the Mo_2C-doped cermets was higher than for the WC cermets, as shown in Fig. 3(b), (c), (e) and (f). Since the atomic radius of W and Mo was the same, i.e. 139 pm, the larger peak shift implies the solubility of Mo in NbC and Ni was higher than for W, as confirmed by the calculations presented in Fig. 2(c) and (d).

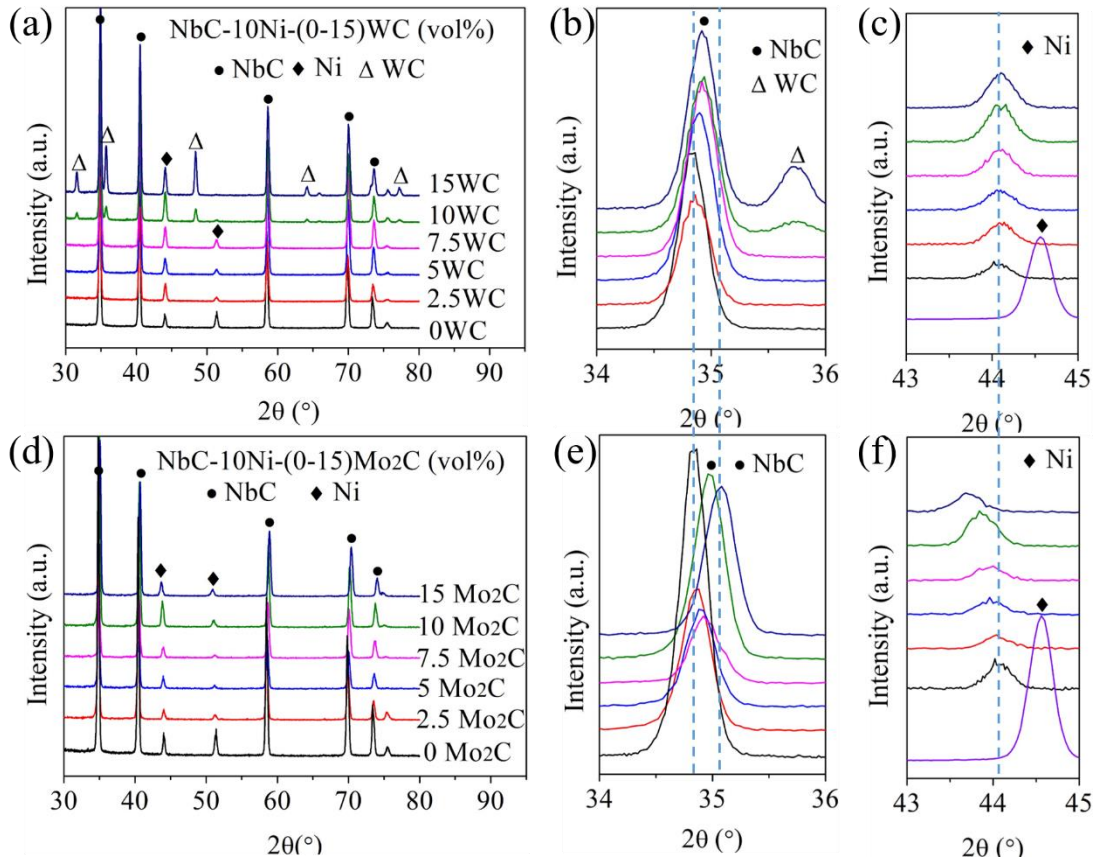

Fig. 3. XRD patterns of the WC (a), (b), (c) and Mo_2C (d), (e), (f) doped cermets sintered at 1390 °C for 90 min.

The evolution of the lattice parameters of the carbide and binder phases as a function of the WC/Mo_2C content is presented in Fig. 4(a). The lattice parameter of the NbC phase decreased linearly from 0.44666 to 0.44404 nm with increasing Mo_2C content, and from 0.44696 to 0.44587 nm with increasing WC content up to 10 vol%. At higher WC content, the lattice parameter remained constant implying the formation of a saturated (Nb,W)C solid-solution. The lattice parameter of NbC in the Mo_2C doped cermets decreased constantly with increased Mo_2C addition, indicating the solubility limit of Mo_2C was not reached. Although the lattice parameter of the Ni phase in the WC and Mo_2C doped cermets is higher than for pure Ni (0.35283 nm), it was nearly constant (~ 0.35630 nm) in the NbC-10Ni-xWC cermets and slightly linearly increased to 0.35926 nm in the NbC-10Ni-xMo_2C (vol%) system, indicating that the Mo concentration steadily increased in the Ni metallic binder phase as shown in Fig. 2(c). The evolution of the lattice parameters was confirmed by the EDX point analysis of the constituent phases presented in Fig. 4(b). The solubility of Mo in the Ni binder and (Nb,

Mo)C phase linearly increased, whereas the W content in (Nb,W)C and Ni binder became constant above 7.5 vol% and 5 vol% WC addition respectively.

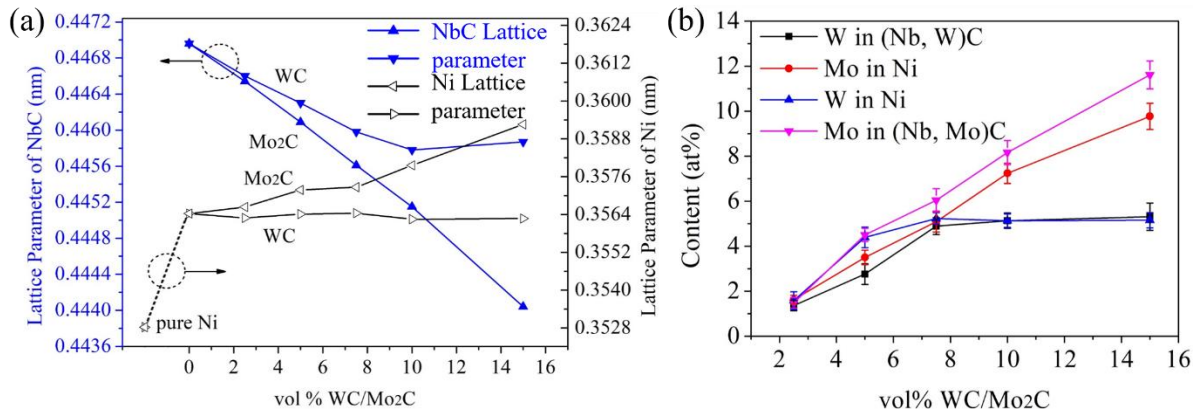

Fig. 4. Lattice parameters of the NbC and Ni phases as a function of the WC and Mo_2C content in the starting powder (a) and evolution of the Mo and W content in the constituent phases, as measured by EDX point analysis (b).

3.3. Microstructural evolution

Backscattered electron (BSE) micrographs of polished surfaces of the cermets doped with different WC compositions sintered at 1390 °C for 90 min are compared in Fig. 5. Three phases were distinguished in the WC doped cermets based on their atomic number contrast. The grey, dark and bright contrast phases were the (Nb,W)C solid solution carbides, Ni binder and undissolved WC. All cermets were obtained by liquid phase sintering according to the Ni binder distribution, in agreement with the thermodynamic prediction shown in Fig. 1(a). The NbC-10Ni-15WC cermet was similar to the TiC-18TiN-24Ni-(10-29)WC (mol%) system where remaining WC was detected after vacuum sintering at 1430 °C for 90 min[18]. Some remaining WC grains were observed in NbC-24.5Co-(10-30)WC cermets[21]. The submicrometer black intragranular spherical spots were small pores or oxygen-rich NbC_xO_y[32]. Comparing Fig. 5(a) with (b) revealed that the solid solution (Nb,W)C grain size was substantially smaller upon adding 2.5 vol% WC, compared to the NbC-Ni cermet. However, ~ 5 vol% WC addition did not show a significant influence on the (Nb,W)C grain growth as shown in Figs. 5(b)-(d). The shape of the NbC grains changed from faceted with rounded corners to rounded as the WC content increased, which indicated that the thermodynamic stability of the solid-solution phase was increased until 10 vol% WC[33].

WC was present in the cermets that contain 10 or 15 vol% WC in the starting powder as shown in Fig. 5(e) and (f), which was consistent with the XRD patterns displayed in Fig. 3(a). The (Nb,W)C grains formed an interconnected carbide grain structure and the Ni solution phase was surrounded by (Nb,W)C grains indicating a reasonably good wettability between (Nb,W)C and the Ni solution phase. A (Nb,W)C core-rim structure with a slightly darker contrast core area was observed in the BSE images of all WC doped cermets. This became more pronounced with increasing WC content. The core/rim boundary appeared rather irregular, which could be explained by interface instability due to the presence of strain energy[34]. Based on the BSE contrast, the core should be richer in Nb whereas the rim should contain more W, as indeed confirmed by the EDX point analysis spectra shown in Fig. 6.

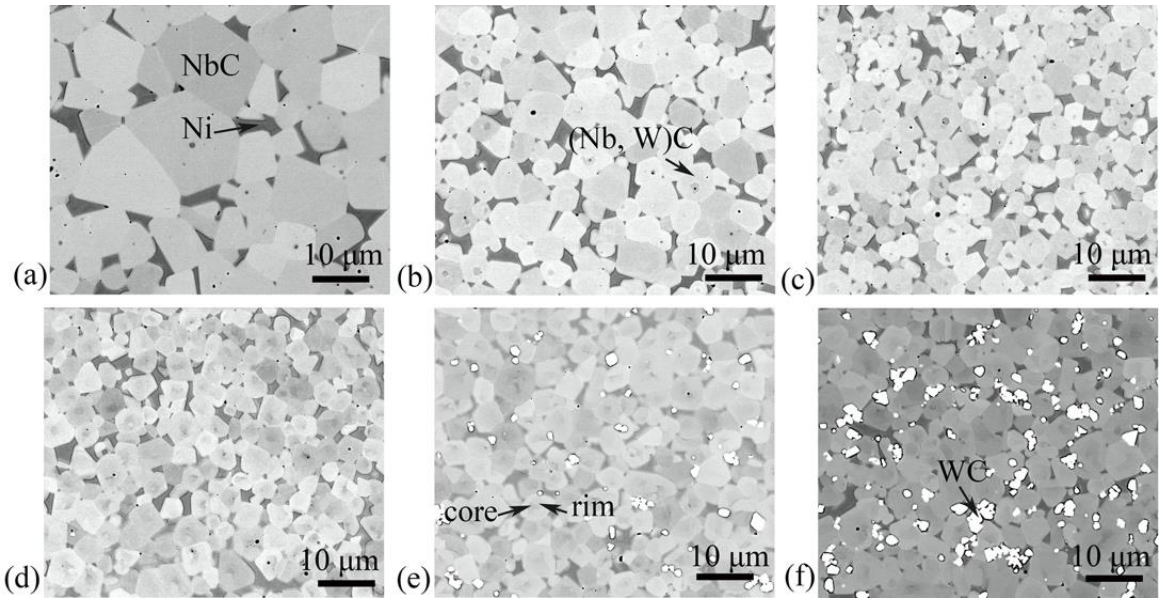

Fig. 5. SEM-BSE micrographs of the cermets with various WC contents: (a) 0; (b) 2.5; (c) 5; (d) 7.5; (e) 10; (f) 15 vol%.

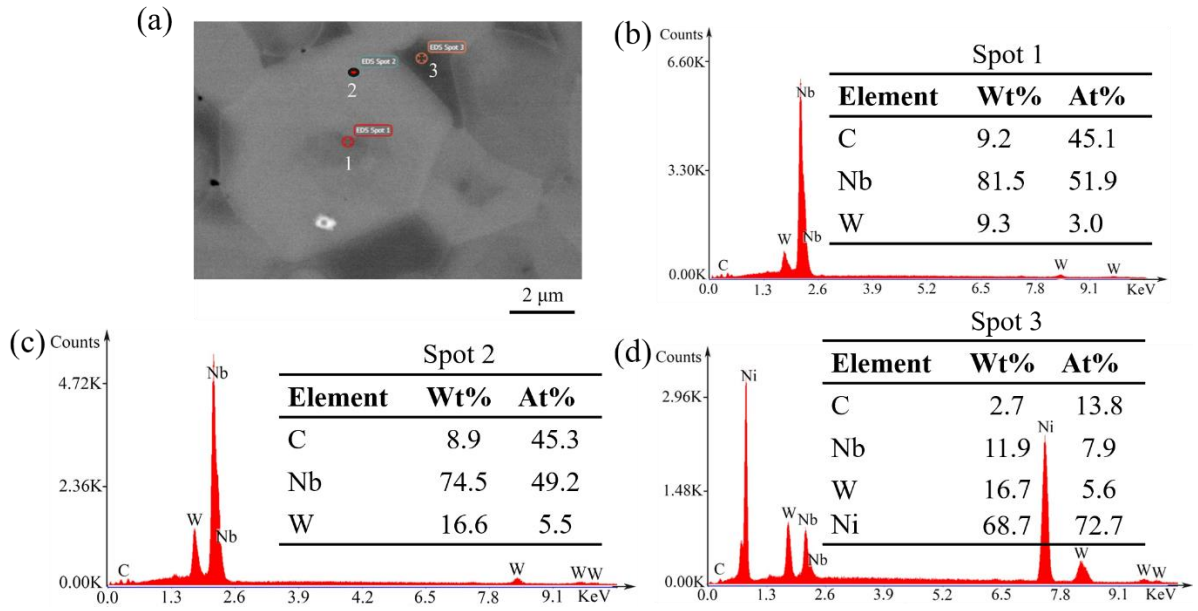

Fig. 6. SEMBSE micrograph revealing the core/rim structure of the (Nb,W)C phase in the NbC-10Ni-7.5WC (vol%) cermet sintered at 1390 °C for 90 min (a), and EDX spectra taken from the core (b), rim (c) and Ni binder (d).

Fig. 7 shows the BSE micrographs of NbC-10Ni-(0-15)Mo_2C (vol%) cermets as a function of the Mo_2C content, sintered at 1390 °C for 90 min. The dark phase was the Ni binder and the grey phase was NbC or (Nb,Mo)C. The (Nb,Mo)C grain size decreased significantly when 2.5 vol% Mo_2C was introduced and varied slightly at ≥ 7.5 vol% Mo_2C where coalescence of some small carbide grains occured. The shape of the NbC grains also changed from faceted with rounded corners to round since the sharp corners were firstly dissolved during liquid phase sintering. More liquid phase was formed at 1390 °C in the cermets with Mo_2C addition than in the WC doped cermets (see Fig.1). In addition, Mo_2C was reported to have the best wettability with Ni compared to other carbides[41], so (Nb,Mo)C had a better wettability with Ni than (Nb,W)C, and the solubility of Mo in NbC was higher than for W. Therefore, no core-rim structure was formed in the Mo_2C doped cermets, indicating a homogeneous solid solution might have been formed already in the solid state. It was reported that Mo_2C additions have a clear inhibiting effect on NbC grain growth, already in the solid state[27]. However, further work is still in progress to understand the mechanisms of grain growth inhibition. Similarly, there was also no core-rim structure in the hard phase of the (Ti,W)C-Ni or (Ti,W)(CN)-Ni system in the size ranges of 100-500 and 200-800 nm, respectively[35]. The contact angle of NbC and Ni at 1420 °C was 11°[36] and decreased

due to a decreased solid-liquid interface energy upon introducing WC or Mo_2C[37]. This interface was expected to suppress carbide growth by inhibiting the coalescence of carbides[38].

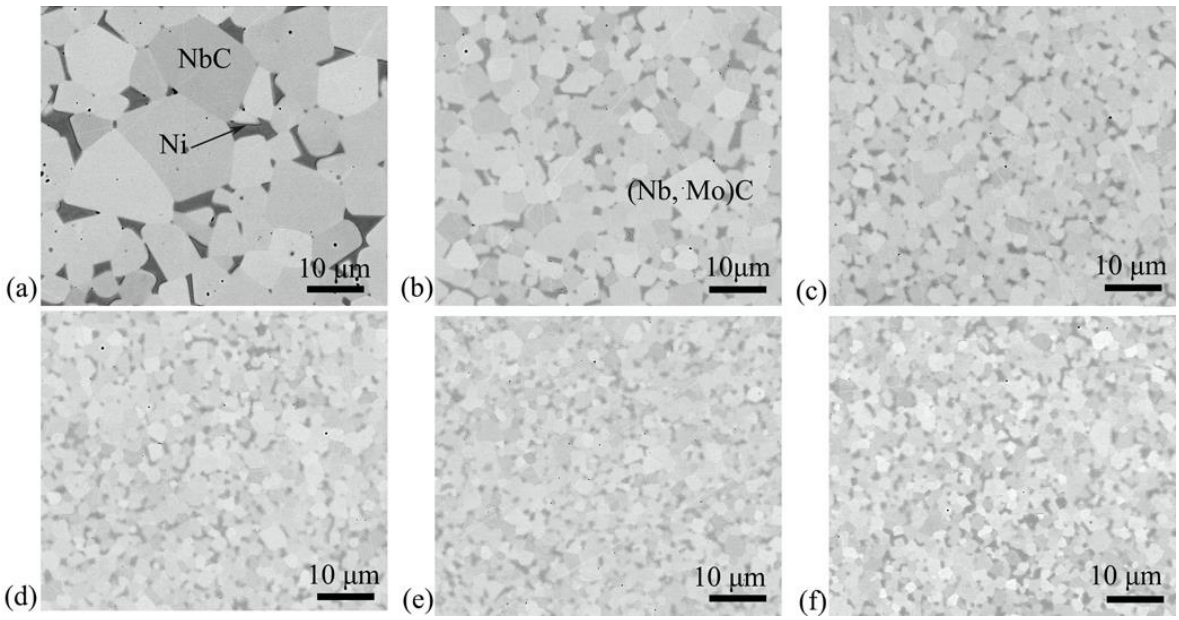

Fig. 7. SEM-BSE micrographs of the cermets with various Mo_2C contents: (a) 0; (b) 2.5; (c) 5; (d) 7.5; (e) 10; (f) 15 vol%.

EBSD maps of NbC-10Ni-7.5WC/Mo_2C (vol%) are shown in Fig. 8. Comparing Fig. 8(a) and (c), a much finer microstructure was observed in the Mo_2C doped cermet. Additionally, the Ni binder distribution was more homogeneous in the Mo_2C doped cermet as shown in Fig. 8(b) and (e).

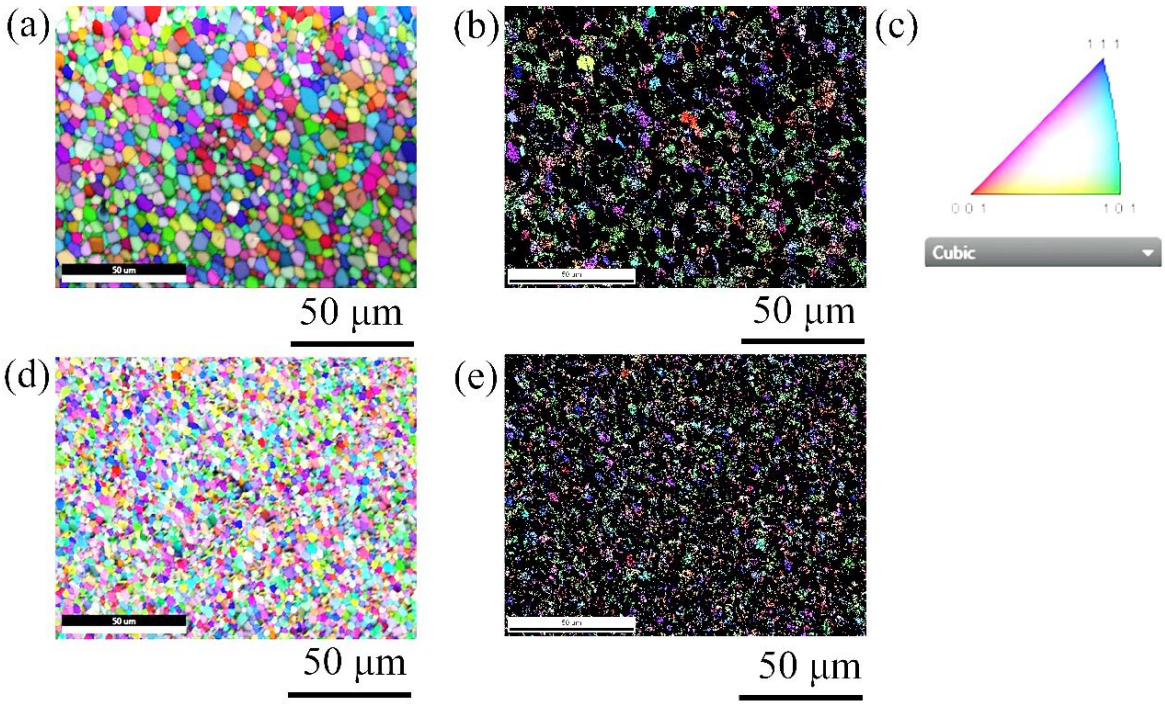

Fig.8. EBSD orientation maps using IPF colouring for the NbC (a,d) and Ni (b,e) phase in the (a,b) NbC-10Ni-7.5WC and (d,e) NbC-10Ni-7.5Mo_2C cermets. (c) color code for Ni binder and NbC phase.

The core-rim evolution with WC content in WC doped cermets is schematically presented in Fig. 9. Only a few core-rim structures were observed in the 2.5 vol% WC doped cermets. The (Nb,W)C solid-solution phases form during sintering when WC was added to NbC-Ni powder and the composition of the (Nb,W)C phase depends mainly on the dissolution rate, the volume fraction, and the surface area of the NbC and WC phases[39]. A similar microstructure evolution was reported for $(Ti_{0.93}W_{0.07})$C-20Ni-(0-25)WC (wt%) and NbC-24.5Co-(4-30)WC (wt%) cermets where the core-rim structure was formed when WC is introduced[21,40]. Free WC was located at the (Nb,W)C/Ni or (Nb,W)C/(Nb,W)C grain boundaries as shown in Fig.9(e) and (f).

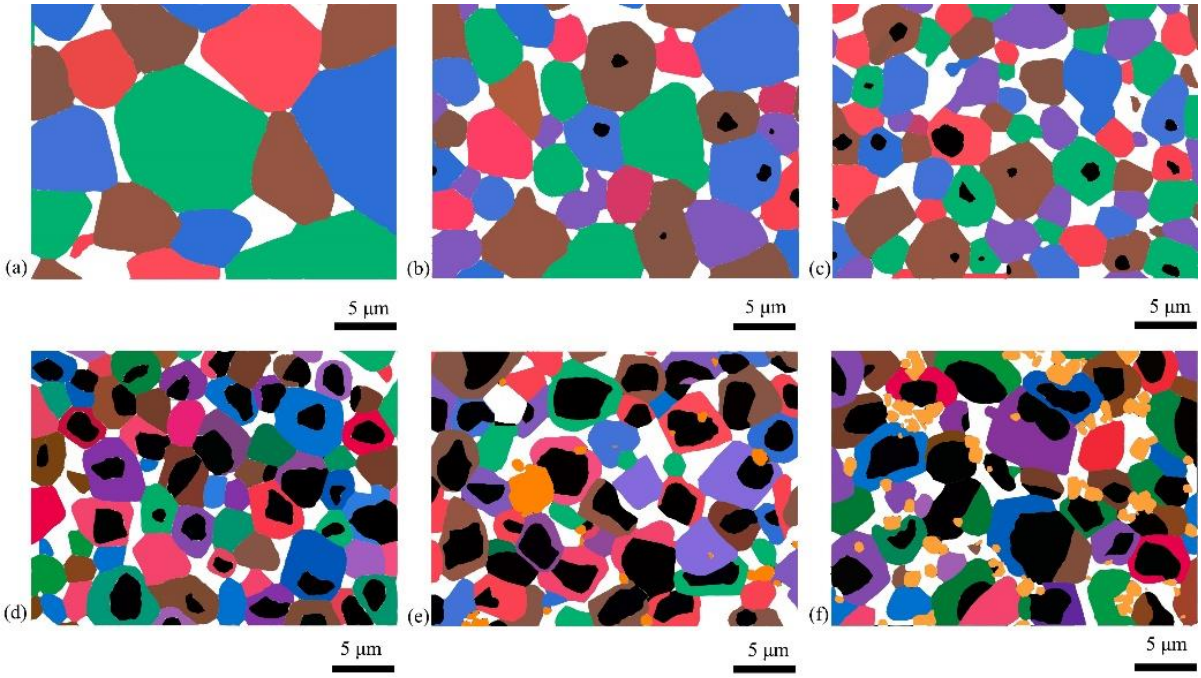

Fig. 9. Schematic representation of the BSE core-rim structure evolution in the NbC-Ni-WC cermets as a function of the WC content; (a) 0; (b) 2.5; (c) 5; (d) 7.5; (e) 10; (f) 15 vol% WC. The orange and white colours represented the WC and Ni binder phase respectively, whereas the core of a core-rim grain is coloured black and the rim or core-less (Nb,W)C grains are coloured.

The average grain size of the (Nb,W)C phase decreased from 3.06 μm to 1.57 μm when 2.5 vol% WC is introduced and levelled off at 1.60 μm with increasing WC content, as shown in Fig. 10(a). This indicated that the grain growth in WC doped cermets was not strongly related to the composition, but rather linked to the kinetics of dissolution and reprecipitation[41, 42]. The average grain size of the (Nb,Mo)C phase grains decreased from 3.06 μm to 1.55 μm with 2.5 vol% Mo_2C addition and slightly decreased to 1.06 μm upon increasing the Mo_2C content to 15 vol%. The average grain size reduction of the carbide solid solution grains was more pronounced in Mo_2C doped cermets than for WC doped cermets. The (Nb,Mo)C had a better wettability with the Ni metallic binder phase than (Nb,W)C, since Mo_2C had the best wettability with Ni amongst all IVB, VB and VIB carbides[43]. Therefore, a finer microstructure was observed in Mo_2C doped cermets as presented in Fig. 7(a)-(f). A similar phenomenon was observed in TiC and Ti(C,N) cermets[17,18]. The grain growth inhibiting effect increased with increasing additive content in the liquid phase until the solubility limit of

the secondary carbides was reached[44]. As described above, the solubility limit of Mo-$_2$C was not reached even at 15 vol% Mo_2C, so Mo_2C kept on decreasing the (Nb,Mo)C grain size, whereas the maximum WC solubility in the nickel binder was already reached at 2.5 vol% WC addition. The Ni binder intercept length decreased from 2.36 µm to 0.79 µm and 0.70 µm, upon 2.5 vol% WC/Mo_2C addition and was nearly constant at 0.52 µm upon increasing the WC/Mo_2C content to 15 vol%. The core-width and rim thickness of the core-rim carbide grains evolved as a function of the WC content as shown in Fig. 10(b). The (Nb,W)C core had already formed during solid state sintering and the rim phase grew around on top by dissolution and reprecipitation of the (Nb,W)C phase in the liquid phase. The amount of (Nb,W)C increased with increasing WC content. The core width increased with increasing WC content until the solid solution limit of WC was reached, which induced decreased rim thickness. The core width increased from 0.30 to 1.15 µm at 10 vol% WC and levelled off with increasing WC content, whereas the rim thickness decreased from 0.98 to 0.29 µm at 10 vol% WC and levelled off with increasing WC content as shown in Fig. 10(b).

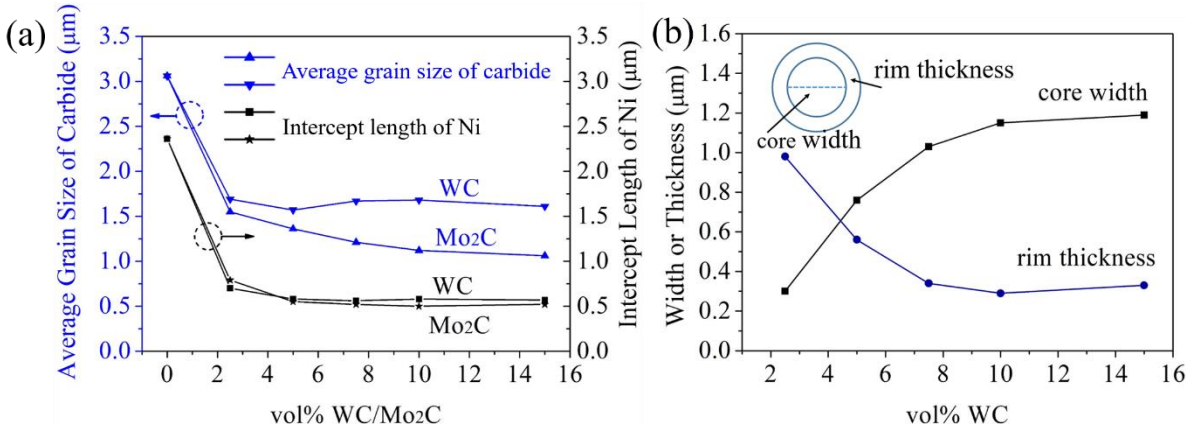

Fig. 10. Average grain size and intercept length versus WC/Mo_2C content (a), and core width and rim thickness as a function of the WC content (b).

The core-rim evolution as a function of the sintering temperature in the 15vol% WC doped cermet is presented in Fig. 11. No core-rim structure was observed in the cermets solid state sintered at 1200 °C or 1280 °C for 90 min as shown in Fig.11(a) and (b). Very few core-rim structures and a large number of Ni agglomerates were observed when sintered at 1330 °C for 90 min. When liquid phase sintering, the dissolution-precipitation process became active, leading to a distinct core-rim structure. Thisbecame obvious when sintering at 1390 °C for 90 min as displayed in Fig. 11(d).

When sintering at even higher temperatures, the core-rim structure gradually disappeared as shown in Fig.11(e) and (f). No residual WC was observed in the 15 vol% WC doped cermet sintered at 1600 °C for 90 min, as confirming by the XRD analysis shown in Fig. 12. The grains became coarse with a less distinct core-rim structure after sintering at 1600 °C because the higher temperature was beneficial for W atom interdiffusion between the core and rim, leading to a smaller black cores with thicker rim phases. Therefore, the final morphology of the cermet tended to become a homogeneous (Nb,W)C solid solution embedded in a Ni-based binder with increasing sintering temperature. A similar phenomenon was observed in the TiC-25WC-11Mo2C-10Ni-8Co-1C (wt%) system[45]. The calculated NbC phase composition in WC/Mo_2C doped cermets as a function of temperature is shown in Fig. 13. The amount of WC dissolved in NbC steadily increased with temperature until 1306 °C, followed by an abrupt increase between 1306 and 1321 °C (as indicated by the dashed circles) and a further increase to level off around 1420 °C (see Fig. 13(a)). Conversely the amount of dissolved Mo_2C is increased with increasing temperature up to 1371 °C and then varies slightly as displayed in Fig. 13(b). There were still core rim structures in the NbC-Ni-15WC (vol%) system even when sintered at 1600 °C for 90 min indicating that the interdiffusion between core and rim was extremely slow. Therefore, the obvious core rim structure was observed after sintering at 1390 °C.

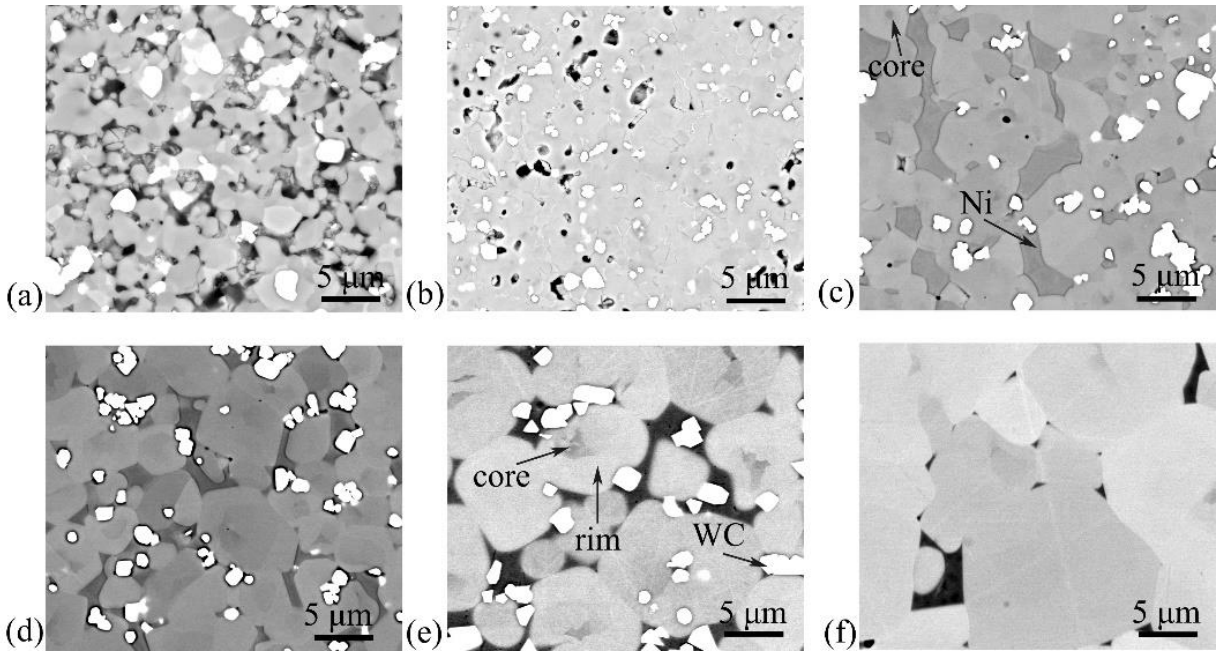

Fig. 11. NbC-10Ni-15WC starting powder sintered at different temperatures: (a) 1200 °C; (b) 1280 °C; (c) 1330 °C; (d) 1390 °C; (e) 1480 °C; and (f) 1600 °C.

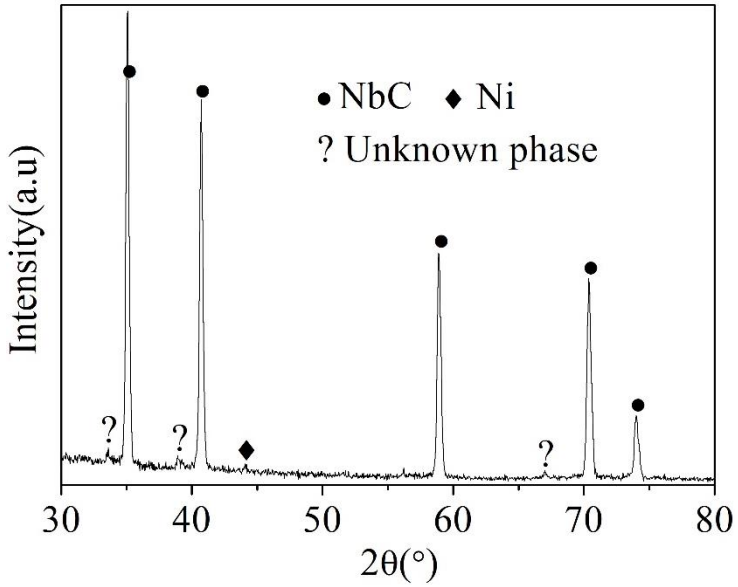

Fig. 12. XRD pattern of the NbC-10Ni-15WC (vol%) cermet sintered at 1600 °C for 90 min.

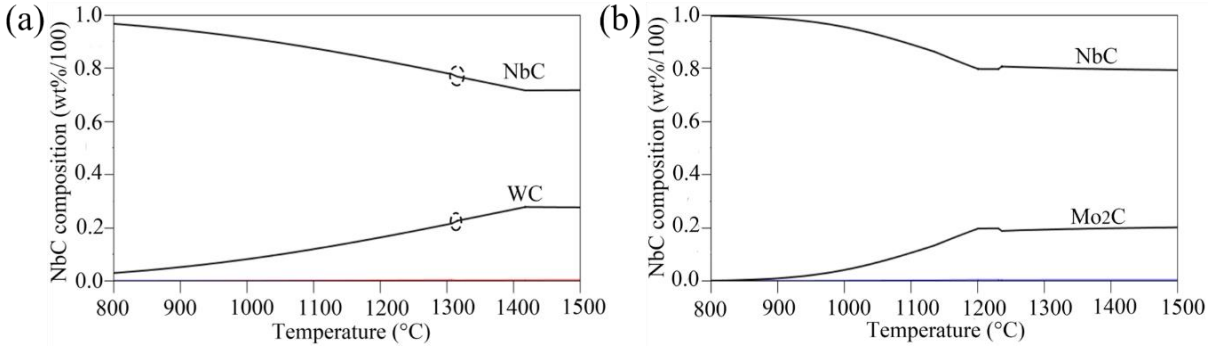

Fig. 13. Calculated NbC phase compositions in the 15 vol% WC/Mo_2C doped cermets as a function of temperature.

Fig. 14 shows BSE images of the 15 vol% WC cermet sintered at 1390 °C for various sintering times. Less distinct core-rim structures were observed in the cermets sintered at 1390 °C for 0, 180 and 360 min compared to the cermet sintered for 90 min. The interdiffusion between cores and rims occurred during sintering and W atoms diffused into the core with increasing sintering time to achieve more equilibrated composition.

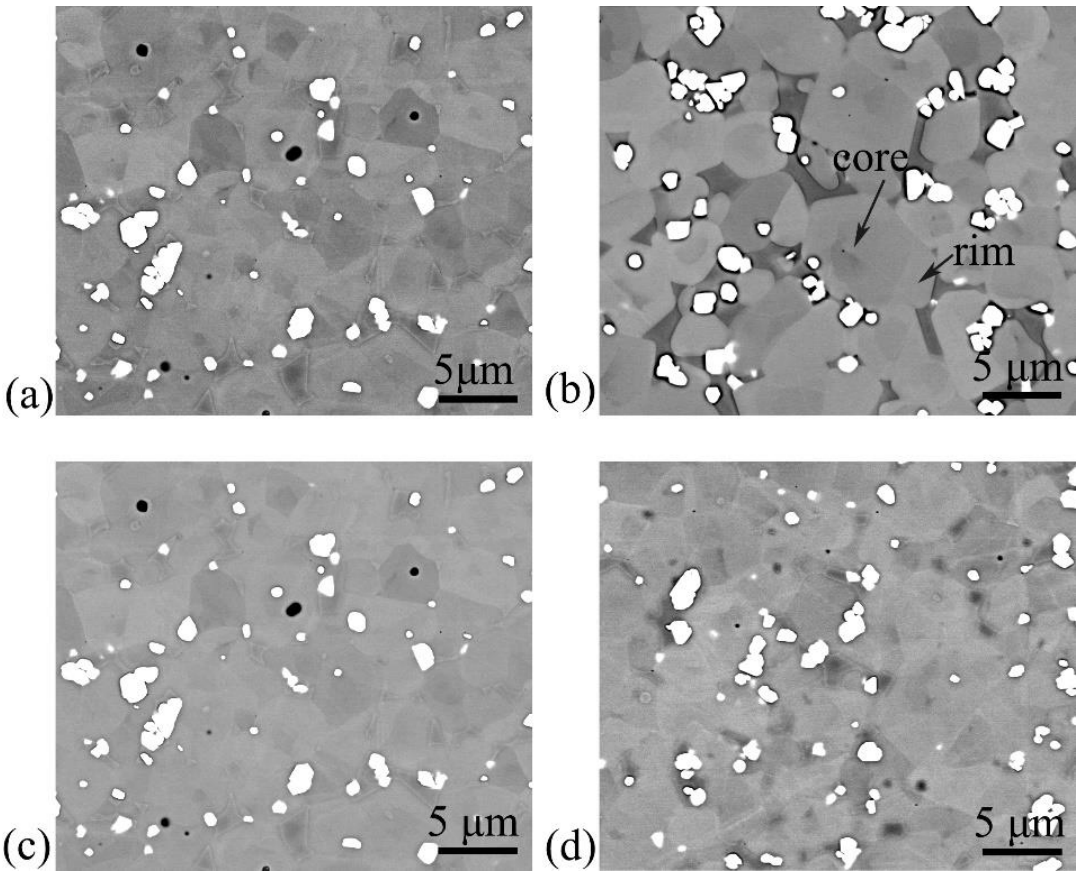

Fig. 14. SEM-BSE micrographs of NbC-10Ni-15WC (vol%) cermets sintered at 1390 °C for different dwell times: (a) 0 min; (b) 90 min; (c) 180 min; (d) 360 min.

There was a significant increase of WC in the NbC matrix in the temperature range from 1376 to 1396 °C according to the calculations shown in Fig. 13(a). However, the interdiffusion between core and rim was extremely slow. Therefore, the addition of WC in NbC-10Ni-(0-15)WC (vol%) cermets resulted in a core-rim structured material. The formation of the rim was related to the dissolution-reprecipitation process. The (Nb,W)C core was formed via solid solution during solid state sintering as displayed in Fig. 11(a)-(b). The newly solid state formed (Nb,W)C phase and undissolved WC dissolved in the molten Ni binder above the liquidus temperature and a W-richer rim of (Nb,W)C precipitated on top of the non-dissolved (Nb,W) or NbC grains which acted as nucleation sites when the liquid Ni binder was oversaturated during the dwell period and during cooling. The W-richer rim structure had the same crystal structure and similar lattice parameters as the NbC/(Nb,W)C core since the XRD patterns did not show any evidence of peak splitting. The core width increased with increasing WC content since larger solid state formed (Nb,W)C grains acted as reprecipitation sites, as presented in Fig.11(b), which caused more core rim structure with increasing WC

content until the solid solution limit of WC was reached as shown in Fig. 9(b)-(f). At higher sintering temperature - longer sintering time combinations, the interdiffusion of W from rim to core led to a more homogeneous (Nb,W)C phase, as shown in Fig. 11 and Fig. 14.

3.4. Mechanical properties

The change in the Vickers hardness and fracture toughness was presented in Fig. 15(a). The Vickers hardness initially increased upon adding 2.5 vol% WC, but levelled off at WC contents of 5-10 vol%, in agreement with the evolution of the (Nb,W)C grain size, as shown in Fig. 11(a). Since the hardness did not change upon 2.5-10 vol% WC addition, the intrinsic hardness of the NbC and (Nb,W)C phases were comparable. A highest HV_{30} of 1261$\pm$ 5.1 kg/mm^2 was measured for the 15 vol% WC grade, which was slightly higher than for the other WC-doped grades most probably due to the intrinsically harder WC phase present. The Vickers hardness of the Mo_2C doped cermets significantly increased with increasing Mo_2C content. For the cermet with 15 vol% Mo_2C addition, a highest microhardness of 1463 $\pm$ 19 kg/mm^2 was measured, correlating with the smallest (Nb,Mo)C grain size of 1.06 µm. The reason can be twofold: (i) according to the Hall-Petch relationship, the hardness increased with decreasing (Nb,Mo)C grain size; (ii) Nb and Mo were dissolved in the Ni binder[18] as shown in Fig. 2(c) to cause solid-solution hardening, but the effect was not identified[46].

The fracture toughness decreased significantly with increasing amount of WC or Mo_2C from 10.9 MPa m$^{1/2}$ without carbide addition down to 7.7 $\pm$ 0.1 MPa m$^{1/2}$ and 8.6 $\pm$ 0.1 MPa m$^{1/2}$ for the 15 vol% WC and Mo_2C doped cermets respectively. The evolution of the contiguity with WC/Mo_2C content is shown in Fig. 15(b). It increased from 0.50 $\pm$ 0.05 with increasing WC/Mo_2C content to a maximum of 0.72 $\pm$ 0.05 and 0.63 $\pm$ 0.04 at 15 vol% WC and Mo_2C addition, respectively. The contiguity for the Mo_2C doped cermets slightly increased between 0 and 2.5 vol% Mo_2C addition, and was constant at 0.63 at higher Mo_2C contents. Above 8 vol% secondary carbide addition, the contiguity in the Mo_2C system was lower than in the WC system, confirming the better wettability in the Mo_2C containing cermets. Due to the higher contiguity, a lower fracture toughness was observed for the WC doped cermets. The

hardness of the WC doped cermets slightly increased with increasing contiguity, while the fracture toughness followed the opposite trend.

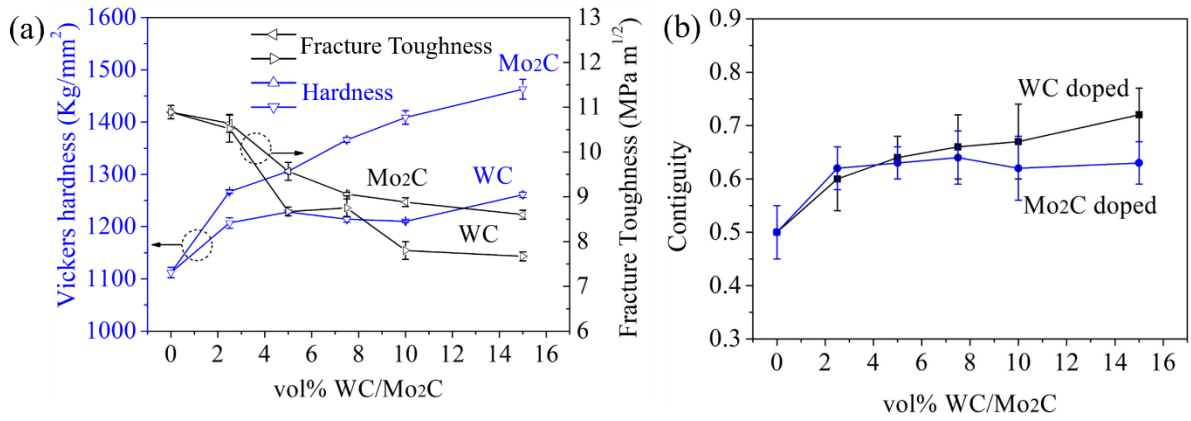

Fig.15. Vickers hardness and indentation fracture toughness (a) and contiguity (b) of the sintered cermets.

The crack propagation path testing with a load of 30 kg during 15 s in the cermets is shown in Fig. 16(a), revealing that the cracks mainly propagated intergranularly along the NbC-Ni interfaces in the NbC-Ni cermet. Cracks mainly propagated along the outer rim grain boundary in WC doped cermets as shown in Fig. 16(c). Both transgranular and intergranular crack propagation were observed in the WC and Mo_2C doped cermets as shown in Fig.16. The Ni binder played a similar role as Co in WC-Co hardmetals, inhibiting crack propagation in the hardmetal by shielding the stress field in front of the crack tip or by forming bridging ligaments behind the crack tip[47]. The similar phenomenon was observed in NbC-Al_2O_3 system[48].

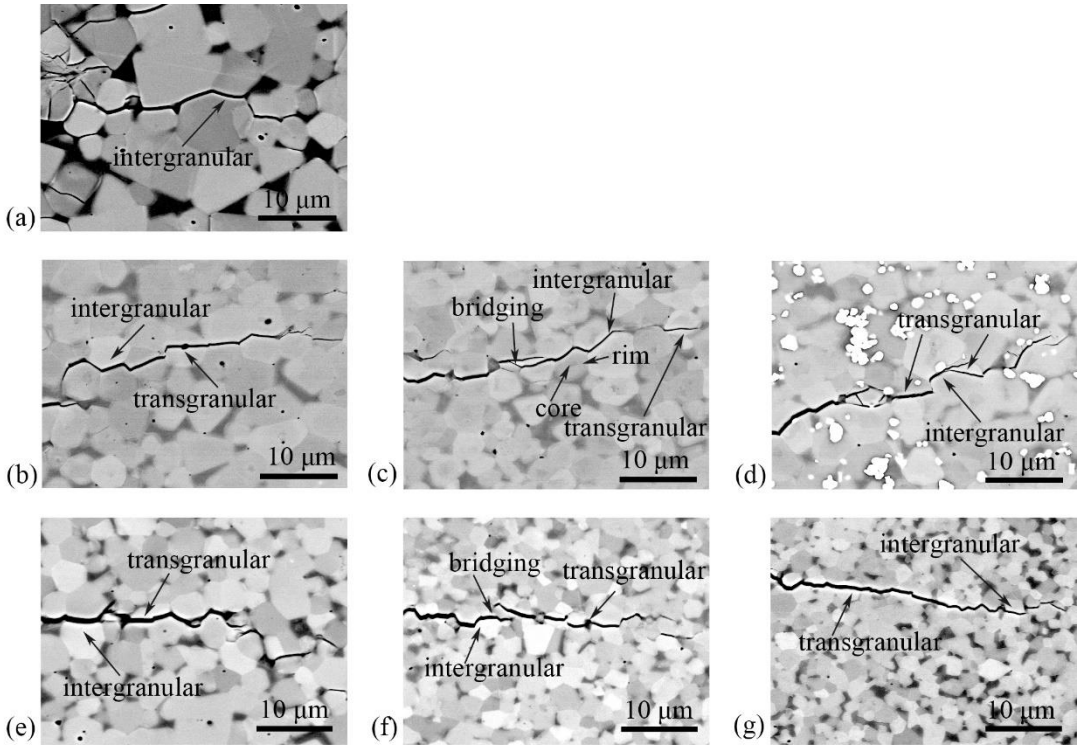

Fig.16. Crack propagation path in the NbC-10Ni-xWC cermets with (a) 0; (b) 2.5; (c) 7.5 and (d) 15 vol% WC; and NbC-10Ni-xMo_2C cermets with (e) 2.5; (f) 7.5 and (g) 15 vol% Mo_2C.

The flexural strength of the cermets with varying WC/Mo_2C content is shown in Fig. 17. The flexural strength initially increased with increasing WC content up to a maximum of 1706 ± 44 MPa at 7.5 vol% WC and was reduced upon further increasing the WC content. The flexural strength of all Mo_2C doped cermets was comparable around 1406 ± 107 MPa, with a highest value of 1482 ± 137 MPa at 5 vol% Mo_2C. According to the Griffith equation (2), the calculated critical flaw size in the 5 vol% Mo_2C doped cermets was about 26 μm which was much largger than the average grain size, implying the (Nb,Mo)C grain refining effect on the flexural strength is limited:

$$\sigma_f = \frac{K_{IC}}{\sqrt{\pi C}} \tag{2}$$

where σ_f is the flexural strength required to propagate a crack of half-length *C* and K_{IC} is the fracture toughness.

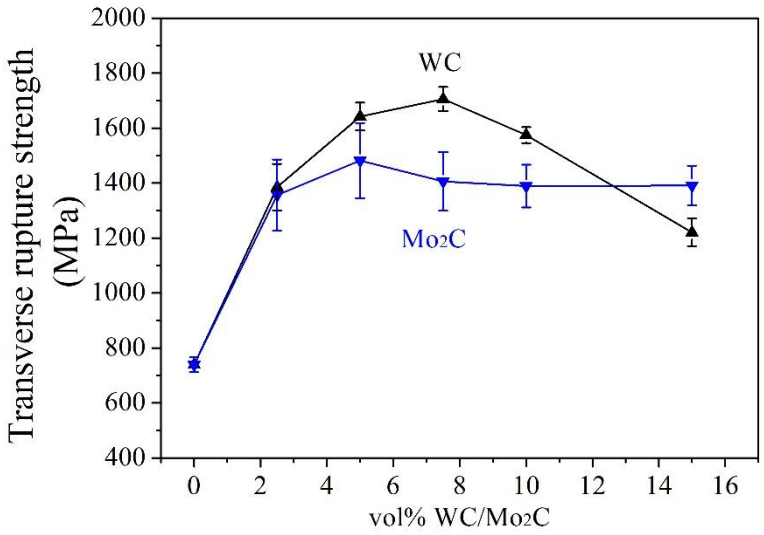

Fig. 17. Transverse rupture strength of the sintered cermets.

4. Conclusions

Fully dense Ni-bonded NbC cermets with up to 15 vol% WC/Mo_2C were synthesized by pressureless liquid phase sintering for 90 min at 1390 °C. XRD lattice parameter analysis, energy dispersive point analysis and Thermo-Calc calculations revealed that the WC or Mo_2C addition mainly dissolved in the NbC phase, forming solid solution (Nb,W)C/(Nb,Mo)C carbide phases, and to a minor extent in the Ni-binder. Residual WC was observed at 10 vol% WC addition, whereas up to 15 vol% Mo_2C completely dissolved into the NbC/Ni cermets.

The liquid phase sintered Mo_2C doped cermets had a finer homogeneous grain sized microstructure, whereas the near solid state sintered WC-containing cermets had a coarser core-rim structured carbide phase with a W-rich (Nb,W)C rim around a Nb-rich (Nb,W)C core. The grain size of the (Nb,Mo)C grains slightly decreased with increasing Mo_2C content above 2.5 vol% resulting in a hardness increase up to 1463 $\pm$ 19 kg/mm^2 (15 vol% Mo_2C addition), whereas the core-rim (Nb,W)C grain size remained constant resulting in a hardness of 1200-1250 kg/mm^2. The contiguity of the WC cermets increased linearly with increasing WC content, accompanied by decreased fracture toughness. The contiguity of the Mo_2C doped cermets kept rather constant around 0.63 $\pm$ 19 at and above 2.5 vol% Mo_2C addition. The Mo_2C-containing cermets however had a higher toughness than their WC equivalents since the wettability in the Mo_2C system was higher than for the WC equivalents, as revealed by their lower contiguity at higher secondary phase starting powder additions. The

flexural strength of the NbC-10Ni-xWC cermets was maximum at 1706 ± 44 MPa at 10 vol % WC, whereas the strength of the NbC-10Ni-xMo_2C cermets was comparable with a highest value of 1482 ± 137 MPa at 5 vol% Mo_2C.

Acknowledgements

Jinhua Huang thanks the China Scholarship Council (CSC) for financial support (CSC No. 201808440473). The authors thank the scientific research fund of Flanders, FWO-Vlaanderen, under project G.0772.16N, the research fund of KU Leuven under project C24-18-061 and the FWO-NSFC international collaboration programme project VS03020N.

References

[1] I. Konyashin, A. Sologubenko, T. Weirich, B. Ries. Complexion at WC-Co grain boundaries of cemented carbides. Mater. Lett. 2017; 187: 7-10.

[2] J. Weidow, S. Norgren and H. O. Andrén. Effect of V, Cr and Mn additions on the microstructure of WC-Co. Int. J. Refract. Met. Hard Mater. 2009; 27: 817–822.

[3] S. Zhang. Titanium carbonitride-based cements: processes and properties. Mater. Sci. Eng A 1993; 163: 141-148.

[4] R. Joost, J. Pirso, M. Viljus, S. Letunovitš and K. Juhani. Recycling of WC-Co hardmetals by oxidation and carbothermal reduction in combination with reactive sintering. Estonian Journal of Engineering 2012; 18(2): 127–139.

[5] W.F. Hastings, P.L.B. Oxley. Predicting tool life from fundamental work material properties and cutting conditions. CIRP Annals 1976; 33–38.

[6] H. Opitz and W. Konig. Proceedings of the 8th International MTDR Conference, 1967, pp. 173-190.

[7] P. K. Wright. Correlation of tool wear mechanisms with slip line fields for cutting in: K. Ludema (Ed.). Wear of Materials. ASME, New York, 1981, pp. 482–488.

[8] M. Woydt, H. Mohrbacher, J. Vleugels, S. Huang, Niobium carbide for wear protection - tailoring its properties by processing and stoichiometry. Met. Powder Rep. 2016; 71(4): 265–272.

[9] L. J. Zhang and Q. Chen. Handbook of Solid State Diffusion, Volume 1. Chapter 6 - CALPHAD-Type Modeling of Diffusion Kinetics in Multicomponent Alloys. 2017.

[10] M. Woydt, S. Huang, J. Vleugels, H. Mohrbacher, E. Cannizza. Potentials of niobium carbide (NbC) as cutting tools and for wear protection. Int. J. Refract. Met. Hard Mater. 2018; 72: 380–387.

[11] F. Qi and S. Kang. A study on microstructural changes in Ti(CN)–NbC–Ni cermets. Mater. Sci. Eng A 1998; 251: 276–285.

[12] S. G. Huang, J. Vleugels, H. Mohrbacher, M. Woydt. NbC grain growth control and mechanical properties of Ni bonded NbC cermets prepared by vacuum liquid phase sintering. Int. J. Refract. Met. Hard Mater. 2018; 72: 63–70.

[13] S. G. Huang, J. Vleugels, H. Mohrbacher and M. Woydt. Microstructure and mechanical properties of NbC matrix cermets using Ni containing metal binder. Met. Powder Rep. 2016; 71: 349-355.

[14] S. G. Huang, J. Vleugels, H. Mohrbacher, M. Woydt. Microstructure and tribological performance of NbC-Ni cermets modified by VC and Mo_2C. Int. J. Refract. Met. Hard Mater 2017. 66: 188–197.

[15] S. G. Huang, K. Vanmeensel, H. Mohrbacher, M. Woydt, J. Vleugels. Microstructure and mechanical properties of NbC-matrix hardmetals with secondary carbide addition and different metal binders. Int. J. Refract. Met. Hard Mater. 2015; 48: 418–426.

[16] M. Woydt, H. Mohrbacher, J. Vleugels, S. Huang, Niobium carbide for wear protection– tailoring its properties by processing and stoichiometry. Met. Powder Rep. 2016; 71(4): 265–272.

[17] N. Liu, Y. Xu, Z. Li, et al. Influence of molybdenum addition on the microstructure and mechanical properties of TiC-based cermets with nano-TiN modification. Ceram. Int. 2003; 29(8): 919-925.

[18] P. Lindahl, P. Gustafson, U. Rolander, et al. Microstructure of model cermets with high Mo or W content. Int. J. Refract. Met. Hard Mater.1999; 17(6):411-421.

[19] J. Jung and S. Kang. Effect of Nano-Size Powders on the Microstructure of Ti(C,N)-xWC-Ni Cermets. Progress in Nanotechnology. John Wiley & Sons, Inc. 2014.

[20] D. Mari, L. Miguel, C. Nebel. Comprehensive Hard Materials. Section III Synthesis and Processing 2014, pp: 240-241.

[21] S.G. Huang, L. Li, O. Van der Biest, J. Vleugels. Influence of WC addition on the microstructure and mechanical properties of NbC–Co cermets. J. Alloys Compd. 2007; 430: 158–164.

[22] M. Woydt, H. Mohrbacher. The tribological and mechanical properties of niobium carbides (NbC) bonded with cobalt or Fe_3Al. Wear 2014; 321: 1-7.

[23] M. Woydt, S. Huang, J. Vleugels, H. Mohrbacher, E. Cannizza. Potentials of niobium carbide (NbC) as cutting tools and for wear protection. Int. J. Refract. Met. Hard Mater. 2018; 72: 380–387.

[24] T. Lapauw, B. Tunca, D. Potashnikov, A. Pesach, O. Ozeri, J. Vleugels, K. Lambrinou. The double solid solution $(Zr, Nb)_2(Al, Sn)C$ MAX phase: a steric stability approach. Sci. Rep. 2018; 8(1): 12801-.

[25] D. K. Shetty, I. G. Wright, P. N. Mincer, A. H. Clauer. Indentation fracture of WC–Co cermets. J. Mater. Res. 1985; 20: 1873–1882.

[26] C. S. Smith and L. Guttman. Measurement of internal boundaries in three-dimensional structures by random sectioning. Trans. AIME 1953; 197: 81-87.

[27] M. Labonne, J. M. Missiaen, S. Lay, N. García, O. Lavigne, L. F. García, E. Tarrés. Sintering behavior and microstructural evolution of NbC-Ni cemented carbides with Mo_2C additions. Int. J. Refract. Met. Hard Mater. 2020; 92: 105295.

[28] P. Ettmayer, H. Kolaska, W. Lengauer, K. Dreyer, Ti(C,N) cermets-Metallurgy and properties. Int. J. Refract. Met. Hard Mater. 1995; 13: 343-351.

[29] I. A. Alhomoudi, G. Newaz. Residual stresses and Raman shift relation in anatase TiO_2 thin film. Thin Solid Films 2009; 517: 4372-4378.

[30] J. D. Makinson, J. S. Lee, S. H. Magner, R. J. De Angelis, W. N. Weins, and A. S. Hieronymus. X-Ray Diffraction Signatures of Defects in Nanocrystalline Materials. JCPDS-International Centre for Diffraction Data 2000, Advances in X-ray Analysis. 42: 1097-0002.

[31] H.-O. Andrén, Rolander U , Lindahl P. Phase composition in cemented carbides and cermets. Int. J. Refract. Met. Hard Mater. 1994; 12(3):107-113.

[32] A. Gupta, O.P. Pandey. NbC/C heterojunction for efficient photodegradation of methylene blue under visible irradiation. Sol. Energy 2019; 183: 398–409.

[33] J. Kim, M. Seo, S. Kang. Microstructure and mechanical properties of Ti-based solid-solution cermets. Mater. Sci. Eng A 2011, 528(6): 2517-2521.

[34] K. W. Chae, D. I. Chun, D. Y. Kim, Y. J. Baik, and K. Y. Eun. Microstructural Evolution During the Infiltration Treatment of Titanium Carbide–Iron Composite. J. Am. Ceram. Soc. 1990; 73(7): 1979-1982.

[35] S. Park, S. Kang. Toughened ultra-fine (Ti,W)(CN)–Ni cermets. Scripta Mater. 2005; 52(2):129-133.

[36] R. Warren. Carbide Grain Growth during the Liquid-Phase Sintering of the Alloys NbC-Fe, NbC-Ni, and NbC-Co. J. Less Common Met. 1969; 17(1): 65-72.

[37] Q. Wang, W. Z. Wang, H. X. Zhang and G. H. Li. Growth kinetics of cermet particles in the form of dissolve separation. Journal of Northeastern University. 1996; 17(5): 490-494.

[38] Laoui T, Zou H, Van der Biest O. Analytical electron microscopy of the core/rim structure in titanium carbonitride cermet. Int. J. Refract. Met. Hard Mater.1992; 11: 207–212.

[39] S. Y. Ahn, S. W. Kim, and S. Kang. Microstructure of Ti(CN)–WC–NbC–Ni Cermets. J. Am. Ceram. Soc. 2001; 84(4):843-849.

[40] J. Kim and S. Kang. Microstructure evolution and mechanical properties of ($Ti_{0.93}W_{0.07}$)C–xWC–20Ni cermets. Mater. Sci. Eng A 2011; 528: 3090-3095.

[41] S. Y. Ahn, S. Kang. Formation of Core/Rim Structures in Ti(C,N)-WC-Ni Cermets via a Dissolution and Precipitation Process. J. Am. Ceram. Soc. 2000; 83(6):1489-1494.

[42] V.G. Zavodinsky. Ab initio study of inhibitors influence on growth of WC crystallites in WC/Co hard alloys. Int. J. Refract. Met. Hard Mater. 2012; 31:263-265.

[43] J. M. Barranco, R. A. Warenchak. Liquid phase sintering of carbides using a nickelmolybdenum alloy. Int. J. Refract. Met. Hard Mater.1989; 6:102–110.

[44] K. Hayashi, Y. Fuke and H. Suzuki. Effects of Addition Carbides on the Grain Size of WC-Co Alloy. Journal of the Japan Society of Powder and Powder Metallurgy, 19, 67-71.

[45] H.W. Xionga, Z. Y. Lia, X.P. Gan, L. Y. Chai. Morphology evolution of TiC-based cermets via different sintering schedules. Ceram. Int. 2017; 43: 5805-5812.

[46] Y. Li , N. Liu, X.B. Zhang, C.L. Rong. Effect of Mo addition on the microstructure and mechanical properties of ultra-fine grade TiC–TiN–WC–Mo_2C–Co cermets. Int. J. Refract. Met. Hard Mater. 2008; 26(3):190-196.

[47] L.S. Sigl, H.F. Fischmeister. On the fracture toughness of cemented carbides. Acta Metall. 1988; 36: 887–897.

[48] L.R.R. Alecrim, J.A. Ferreira, C.F. Gutiérrez-González, M.D. Salvador, A. Borrell, E.M.J.A. Pallone. Effect of reinforcement NbC phase on the mechanical properties of Al_2O_3-NbC nanocomposites obtained by spark plasma sintering. Int. J. Refract. Met. Hard Mater.2017; 64: 255–260.